A novel bivalent anti-c-MET/PD-1 bispecific antibody exhibits potent cytotoxicity against c-MET/PD-L1-positive colorectal cancer

Zujun Sun
Tongji University
Chenzheng Gu
Tongji University
Xuan Wang
Tongji University
Anquan Shang
Tongji University
Wenqiang Quan
Tongji University
Junlu Wu
Tongji University
Ping Ji
Tongji University
Yiwen Yao
Tongji University
Wenfang Liu
Tongji University
Dong Li (lidong@tongji.edu.cn)
Tongji University

Research Article

Keywords: Colorectal cancer, Bispecific antibody, c-MET, PD-1, Focal adhesion kinase, GRB2-associated-binding protein 1

Posted Date: April 8th, 2022

DOI: https://doi.org/10.21203/rs.3.rs-1528415/v1

Abstract

Previously, we generated a novel bispecific antibody (BsAb) targeting c-MET and PD-1 (PDCD1), which can bridge T cells and c-MET positive tumor cells. This study investigated functional mechanisms and antitumor activities of our BsAb against c-MET/PD-L1 (CD274) positive colorectal cancer (CRC). The Cancer Genome Atlas database was used to evaluate c-MET expression in tumor tissues. The expression of plasma exosomal c-MET/PD-L1 in CRC patients was measured by enzyme-linked immunosorbent assays. Western blotting assay was performed to determine expression levels of c-MET and molecular mechanism. The scratch wound healing migration assay and transwell chamber invasion assay were conducted to determine cell migratory and invasive abilities, respectively. A humanized mouse model was used to evaluate antitumor activity of the BsAb *in vivo.* The BsAb inhibited c-MET/PD-L1$^+$ CRC cell migration and invasion and mediated strong antitumor activity against HCT116 tumors in mice. The BsAb induced the degradation of c-MET protein in a dose and time-dependent manner. The BsAb suppressed the phosphorylation of c-MET downstream proteins GRB2-associated-binding protein 1 (Gab1) and focal adhesion kinase (FAK). The BsAb promoted macrophage phagocytosis. Furthermore, the level of plasma exosomal-c-MET/PD-L1 distinguished CRC patients from healthy controls. The BsAb exhibited potent anti-tumor activities by two distinguished mechanisms: inhibition of c-MET signal transduction and promotion of macrophage-mediated phagocytosis. Our BsAb may provide a novel therapeutic tool for patients with c-MET/PD-L1$^+$ CRC, and the status of exosomal-c-MET/PD-L1 may be predictive responsiveness to treatment with our BsAb.

Introduction

Colorectal cancer (CRC) is one of the most common gastrointestinal malignancies and the fourth leading cause of cancer-related death worldwide [1]. Currently, the treatment for CRC is surgery plus chemotherapy and radiotherapy. However, most patients lose the option for surgical treatment because they present with advanced CRC stage at the time of diagnosis with a 5-year survival rate of less than 50% [2]. Consequently, there is an urgent need to find new and effective therapies for patients with CRC, especially for those with advanced cancer.

Immunotherapy has made a breakthrough in the field of tumor therapeutics as an effective adjuvant to surgery, chemotherapy, and radiotherapy. Compared with other conventional therapeutic approaches, immunotherapy has some special advantages, which include alleviating pain, increasing appetite, and significantly improving the quality of life in advanced cancer patients [3]. As traditional immunotherapeutic drugs, monoclonal antibodies have gradually become a main pillar of tumor treatment. Monoclonal antibodies containing the Fc domain retain Fc-mediated effector functions, such as antibody dependent cell-mediated cytotoxicity, complement dependent cytotoxicity, and antibody dependent cellular phagocytosis [4, 5]. Immune checkpoint protein inhibitors, such as antibodies against programmed death (PD) 1 (PDCD1) and PD-ligand 1 (PD-L1) (CD274), have shown to be efficacy against a large number of cancer types, including melanoma, non-small-cell lung cancer and renal cancer. However, even in these cancers, many patients do not benefit from this immunotherapy and only 10–30%

of them respond to anti-PD-1/PD-L1 therapy [6]. At present, the reason for the low response rate is unclear.

Based on the gene sequence of traditional monoclonal antibodies, bispecific antibodies (BsAb) are redesigned and constructed using genetic recombination technology to produce antibodies that target two antigens. With the development of advanced technology, different formats of BsAbs have been proposed. In recent years, some studies have found that BsAbs have better clinical efficacy in the therapy of malignant tumor compared with conventional treatments [7]. BsAbs can target effector cells (T cells, NK cells, macrophages, and monocytes), recruit them to the tumor cells, and enhance tumor killing in a non-MHC-restricted manner [8, 9]. Moreover, BsAbs not only offer an effective linkage between therapeutics and targets, they may also simultaneously block two different oncogenic mediators, e.g. anti-EGFR × anti-HER2 and anti-EGFR × anti-c-MET BsAbs [10, 11]. Therefore, BsAbs have a substantial advantage over traditional monoclonal antibodies with regard to anti-tumor activity, and the clinical treatment benefits are significantly better with a BsAb than a single monoclonal antibody or a combination of two monoclonal antibodies [12, 13].

For anti-PD-1/PD-L1 treatment, recent data suggested that the expression level of PD-L1 in tumor-infiltrating immune cells was a potential biomarker for predicting therapeutic efficacy [14]. One of the key issues for developing c-MET-related therapeutics is the identification of appropriate predictive biomarkers to assess the efficacy of drug treatment. The inhibition of c-MET alone can reduce cellular proliferation in tumors. Several c-MET inhibitors have undergone clinical development for treatment of hepatocellular carcinoma, and c-MET overexpression is a potent predictor of treatment response to c-MET inhibitors [15].

Previously, we designed, expressed and purified a novel BsAb against c-MET and PD-1 that bridges T cells and c-MET positive tumor cells and redirect the T cells to kill the tumor cells [16, 17]. However, the therapeutic activity of this BsAb is unclear and requires a further evaluation of biomarkers that may be useful to predict BsAb treatment outcomes in CRC patients. In this study, we explored functional mechanism and anti-tumor activities of our BsAb against c-MET/PD-L1 positive CRC *in vitro* and *in vivo*. Furthermore, we explored the clinical value of c-MET and PD-L1 status in plasma-derived exosomes, which may serve as predictive biomarkers of response to our BsAb treatment in CRC patients.

Materials And Methods

Database analysis of gene and protein expression profiles

TIMER2 web (http://timer.cistrome.org/), web server (http://gepia2. cancer-pku.cn/#analysis), the UALCAN portal (http://ualcan.path.uab.edu/analysis-prot.html), and TCGA database were used to analyze the expression level of c-MET in primary tumor and normal tissues.

Clinical samples

Human CRC specimens and peripheral blood were obtained from Tongji Hospital, Shanghai, China after obtaining written informed consent from the donors. The study was performed according to the Declaration of Helsinki and was approved by the Institutional Ethics Committee of Tongji Hospital, Shanghai, China (2021-KYSB-061). Excised tumor tissues were paraffin-embedded and sectioned for immunohistochemistry.

Cell lines and cell culture conditions

HCT116, SW480, DLD1, RKO, and THP1 cells were obtained from the ATCC, cultured in DMEM supplemented with 10% FBS (Gibco-Thermo Fisher Scientific) and of 1% penicillin/streptomycin (Gibco). Cells were incubated at 37°C in a humidified incubator containing 5% CO_2.

Reagents and Antibodies

Human recombinant HGF was purchased from GenScript Biotech (Z03229, Nanjing, China). The c-MET kinase inhibitors JNJ38877605 was obtained from Selleckchem (S1114, Houston, TX, USA). Antibodies were purchased from Cell Signaling Technology, Inc. and included antibodies against: c-MET (#8198), phospho-MET (Tyr1234/5) (#3077), phospho-MET (Tyr12349) (#3133), Gab1(#3232), p-Gab1, FAK (#3285), p-FAK (Tyr397) (3283#), PD-1 (#86163), PD-L1 (#85164), GM130 (#12480), Flotillin-1 (#18634), CD9 (#13174), β-actin mAb (#4967). Horse radish peroxidase-conjugated anti-mouse IgG antibody (#7076) was used as a secondary antibody.

RNA isolation and real-time quantitative PCR (qPCR)

Total RNA was isolated from each cell line with TriReagent (Sigma-Aldrich) according to the manufacturer's instructions. The synthesis of cDNA (Sangon Biotech, Shanghai, China) and qPCR reactions were performed using the SYBR® FAST qPCR Kit Master Mix (KAPA, Biosystems). The primer pairs used were as follows: *c-MET*, forward 5'-TTCACCGCGGAAACACCCATC-3', reverse 5'-GTCTTCCAGCCAGG CCCA-3'; *PD-L1*, forward 5'-TGGCATTTGCTGAACGCATTT-3', reverse 5'-GTG GTGGTCTTACCACTCAGG-3'; *CD163*, forward 5'-GACGCATTTGGATGGATC ATGT-3'; reverse 5'-CCCACCGTCCTTGGAATTTGA-3'; *CD206* forward 5'-GGG TTGCTATCACTCTCTATGC-3', reverse 5'-TTTCTTGTCTGTTGCCGTAGT-3'; IL-10 forward 5'-TCAAGGCGCATGTGAACTCC-3', reverse 5'-GATGTCAAACT CACTCATGGCT-3'; *TNF-α* forward 5'-CCTCTCTCTAATCAGCCCTCTG-3' reverse 5'-GAGGACCTGGGAGTAGATGAG-3'; *IL-1β* forward 5'-TGATGG CTTATTACAGTGGCAATG-3', reverse 5'-GTAGTGGTGGTCGGAGATTCG-3'; *IL-12* forward 5'-GGAAGCACGGCAGCAGAATA-3' reverse 5'-AACTTGAGG GAGAAGTAGGAATGG-3'; *GAPGH* forward 5'-GGTGGTCTCCTCTGACTTCAA CAG-3' reverse 5'-GTTGCTGTAGCCAAATTCGTTGT-3'. ΔCT (cycle threshold) values were calculated based on the mean CT values of the target genes and mean CT values of the reference control gene *GAPDH*, using the following formula: ΔCT = Mean CT for Target Gene – Mean CT for *GAPDH*. Relative gene expression levels were calculated using ΔΔCT analysis. ΔΔCT = ΔCT of Sample – ΔCT of Calibrator. Relative Gene Expression = $2^{-(\Delta\Delta CT)}$.

Exosome isolation from plasma and cell culture supernatants

There were 30 CRC patients enrolled for testing and validation studies between March 2021 and July 2021 as well as 20 healthy individuals who were sex and age matched with patients in the testing and validation sets. Detailed clinical data are summarized in supplementary Table 1. The blood samples included in this study were collected in vacuum blood tubes with anticoagulant (EDTA-K2) prior to surgery and pharmacotherapy and centrifuged at 3000 × g for 15 min at 4ºC. The plasma (250 μL) was added to a new tube, to which Exo-Quick™ solution (EXOQ5A-1; SBI System Biosciences, USA) (63 μL) was added. The mixture was mixed, kept at room temperature for 30 min, and then centrifuged at 1500 × g for 30 min. The supernatant was discarded and the pellets were resuspended at 1500 × g for 5 min. The pellets containing total exosomes were resuspended in 100 μL of PBS.

The exosome isolation from cell culture supernatant was performed using differential ultracentrifugation. Briefly, culture cells (100 mL) were centrifuged at 4°C to obtain supernatant, which were subject to centrifuge at 10,000 × g for 20 min. The resulting supernatant were transferred to sterile centrifuge tube and then centrifuged at 100,000 × g at 4°C for 70 min. The supernatant was removed, and the sediments resuspended in 1× PBS/TBS, filter through 0.22 μm strainer, and recentrifuged at 100,000×g for 1 h. The previous step was repeated, and the exosomes were collected.

Transmission electron microscopy

Isolated exosomes were re-suspended in PBS and 20 μL of the suspension was placed on a carbon-coated copper grid and incubated together for 10 min at room temperature. Next, the grid was washed by sterile distilled water, placed in contact with 2% uranyl-oxalate solution for 1 min, and dried for several min. Finally, the grid was observed using an electron microscope (JEM1400, JEOL, Tokyo, Japan).

Nanoparticle tracking analysis

In order to identify the exact size and quantity of isolated particles, the suspension with concentration between 1×10^7/mL and 1×10^9/mL was examined using ZetaView PMX 110 (Particle Metrix, Meerbusch, Germany) equipped with a 405 nm laser. For each suspension, a video of 60 s duration was recorded with a frame rate of 30 frames/s, and particle movement was analyzed using nanoparticle tracking analysis software (ZetaView 8.02.28).

In vitro wound healing assay to measure migration

HCT116 and SW480 cells were added to a 24-well plate. After overnight incubation, a sterile 10 μL pipette tip was used to create a wound across a cell culture monolayer. Cells were incubated in DMEM-0% FBS in the presence of BsAb or the c-MET kinase inhibitor JNJ38877605 for 2 h and were treated with HGF (100 ng/mL). Photographs of the wound were taken immediately after wounding and 24 h using a phase-contrast microscopy. The efficiency of the wound healing process was determined by calculating the area of the cell gap at the indicated times (0 and 24 h) using ImageJ software. Three images were recorded for

each wound at each experimental timepoint. The results are expressed as the percentage of healing at 24 h with respect to the zero timepoint.

Cell invasion assay

Cell invasion assays were performed as previously described [19]. HCT116 and SW480 cells were suspended in serum-free DMEM and then 0.1 mL of each cell line was added to the inserts. Next, 0.7 mL DMEM containing serum with or without BsAb was added to each lower chamber. The chemoattractant was 10% fetal calf serum. The chambers were assembled and incubated for 24 h at 37°C. Non-invading cells were removed from the upper surface of the membrane. The invading cells on the lower surface were fixed with 100% methanol, stained with 0.1% crystal violet solution (Sigma-Aldrich, St. Louis, MO, USA), and counted using five random microscopic fields. The relative migration was calculated based on the ratio of the number of invading cells in the BsAb or JNJ38877605 treatment group versus the number of invaded cells in the control group.

Western blotting

The cells were lysed with M-PER® Mammalian Protein Extraction (Pierce). Proteins were quantified using the BCA Protein Assay kit (Pierce) in accordance with the manufacturer's instructions. Samples containing a total of 50 μg protein were incubated at 100°C for 5 min, separated by SDS-polyacrylamide gel electrophoresis, and subsequently electrotransferred onto polyvinylidene difluoride membrane. Protein detection was performed by overnight incubation with a specific primary antibody at 4°C, incubation with horse radish peroxidase-conjugated secondary antibody (1:5,000 dilution; Pierce Chemical) was added for 1 h at room temperature, and used of a chemiluminescent detection system. Anti-β-actin antibody was used as the control.

Immunohistochemistry

Tumor samples were fixed in 4% formalin, embedded in paraffin, and sectioned into 4-μm-thickness slices. After dewaxing, tissues sections were processed by antigen retrieval, followed by the quenching of endogenous peroxidase activity using hydrogen peroxide. PBS containing 0.1% Tween 20 and goat serum was used to block non-specific binding sites. Slides were incubated with polyclonal antibodies against c-MET. After washing with PBS, slides were incubated with biotinylated anti-rabbit IgG antibody followed by horseradish peroxidase-conjugated streptavidin. After developing in DAB substrates (Invitrogen), 5 high-magnification fields were randomly selected in each slide, and the numbers of positive cells in each field were counted using Image-Pro Plus (Media Cybernetics, Inc.).

Enzyme-linked immunosorbent assay (ELISA)

The quantification of c-MET and PD-L1 in exosomes from cell culture supernatants and plasma was performed by sandwich immunoassay using the Human MET/Hepatocyte Growth Factor Receptor ELISA Kit (RAB0676, Sigma) and Human PD-L1 Sandwich ELISA Kit (KE00074, proteintech). Briefly, 100 μL of each sample was added to the ELISA plate and incubated for 60 min at 37℃. The plate was washed 3

times, and solution B was added. The plate was incubated for 30 min at 37℃, washed 5 times, and 90 μL of substrate was added. After incubating for 15 min at 37℃, 50 μL of termination solution was added, and the plate was immediately analyzed using a spectrophotometer set at a wavelength of 450 nm.

Human peripheral blood mononuclear cell (PBMC) preparation and transplantation

Blood from healthy volunteers was collected in heparinized tubes. The isolation of PBMCs was described as previously [16]. A total of 1×10^8 PBMC per mouse were injected into 5-to 6-week male NOD/SCID mice (SLAC Laboratory Animal Co., Shanghai, China) through tail vein for the reconstitution of immune system.

Tumor xenograft study

Humanized NOD/SCID mice production method was reported as previously (16). All animals were kept in a specific pathogen-free facility and treated in accordance with the National Institutes of Health Care and Use of Laboratory Animals. This study was approved by the Institutional Animal Care and Use Committee of Shanghai Tongji Hospital. For HCT116 xenograft, mice were treated as follows: BsAb (10 mg/kg, intraperitoneal (IP), twice per week), IgG4 and anti-PD-1 (5 mg/kg, IP, twice per week), JNJ-38877605 (20 mg/kg, itragastric gavage, twice per week). PBMCs (1×10^8) were injected into the tail vein on the first and the fourth time drugs were administered. Body weight and tumor size were measured using an electronic balance and a vernier caliper respectively. Tumor volume was calculated using the formula: volume = (length × width^2) × 0.5.

Neutral red analysis

Monolayers of cells were prepared in 24-well plate incubated with 0.1% neutral red physiological saline for 20 min. The supernatant was discarded, and the cells were washed three times with warm PBS to remove unincorporated neutral red particles. The neutral red dye was released from the cells by incubation with 0.2 mL cytosolic solution (50:50 acetic acid: anhydrous ethanol) at room temperature for 2–3 h. After the cells were dissolved, the absorbance was measured using a microplate reader set at 540 nm wavelength.

Statistical analysis

Statistical analysis was performed using SPSS 19.0 statistical software (SPSS, Inc., Chicago, IL, USA) and graphs were generated using GraphPad Prism 5.0. Student’s t-test was used in analyzing differences between the two groups. The p-value of <0.05 was used to evaluate significance of the data.

Results

c-MET gene expression analysis

We input *c-MET* in the “Gene_DE” module of tumor immune estimation resource TIMER2 and observed the differences in *c-MET* expression between tumor and adjacent normal tissues for various tumors or specific tumor subtypes found in the TCGA database. The results showed that *c-MET* expression levels in many cancer tissues were significantly higher than that in the corresponding adjacent tissues, including colon adenocarcinoma (COAD) ($P < 0.001$) and rectum adenocarcinoma (READ) ($P < 0.01$) (Fig. S1).

For certain tumors without normal or with highly limited normal tissues, we used the “Expression analysis-Box Plots” module of the Gene Expression Profiling Interactive Analysis 2 web server to determine *c-MET* expression differences between these tumor and the corresponding normal tissues found in the Genotype Tissue Expression database. We found *c-MET* expression difference between normal and tumor tissues for diffuse large B-cell lymphoma, lower grade brain glioma, skin cutaneous melanoma, testicular germ cell tumors, and thymoma (Fig. S2, $P < 0.05$). However, we did not observe a significant difference for other tumors, such as glioblastoma multiforme, adrenocortical carcinoma, cervical squamous cell carcinoma, endocervical adenocarcinoma, or pancreatic adenocarcinoma (data not shown).

The UALCAN portal is an interactive web resource for analyzing cancer Omics data, and allowed us to analyze protein expression using the Clinical Proteomic Tumor Analysis Consortium (CPTAC) dataset. We compared the expression levels of MET protein (NP_000236.2) between primary tumor and normal tissues by entering “MET”. The available datasets of six tumors were selected, including breast cancer, ovarian cancer, clear cell renal cell carcinoma, colon cancer, uterine corpus endometrial carcinoma, and lung adenocarcinoma (Fig. S3).

The clinical value of c-MET mRNA expression in tumor specimens

Colorectal cancer includes COAD and READ. We used the R Studio to compare *MET* gene expression in COAD and READ tissues and matched adjacent tissues from the TCGA database. Significant increases in *MET* expression were observed in COAD and READ tissues when compared with their corresponding matched adjacent tissues (Fig. 1A). To analyze the expression of *c-MET* as a diagnostic test, a cut-off value was required, which must be reached to consider a sample positive. This value was determined using a receiver operating characteristics (ROC) curve. The resulting diagnostic test showed that there were significant changes in *MET* gene expression in COAD (AUC=0.979; CI95% 0.967-0.990; cut off = 5.039, $P < 0.001$) and READ (AUC=0.935; CI95% 0.864-1.000; cut off = 5.181, $P < 0.001$) in TCGA (Fig. 1B).

The correlation between c-MET gene expression and pathological stages in CRC patient

To further clarify the clinical significance of *c-MET* gene expression in patients with CRC, the TCGA database was used to analyze the correlation between *c-MET* gene expression and age, gender, and M, N, and T CRC stages (Table S2, 3). There was no correlation between *c-MET* gene expression and age or gender (Fig. 2A, B). However, the results indicated that the levels of *c-MET* were higher in M, N, and T staged CRC compared with levels in their respective normal tissues (Fig. 2C–E). To quantitate c-MET protein expression in tumor, a panel of carcinoma tissues and adjacent tissues from CRC patients were

stained using an anti-c-MET antibody. Immunohistochemistry analysis of those specimens revealed that all tumor cells were c-MET positive with scores from 1–3^+, whereas cells in the adjacent tissues were negative, suggesting that c-MET overexpression is tumor-cell specific (Fig. 2F).

BsAb inhibits HGF-stimulated cancer cell invasion and migration

First, we evaluated the expression of c-MET and PD-L1 mRNA in four human cancer cell lines using qPCR. HCT116 and SW480 cell lines expressed *c-MET* mRNA, and four cell lines (HCT116, SW480, DLD1, RKO) expressed *PD-L1* mRNA at relatively high levels (data not shown). Next, we devaluated c-MET and PD-L1 protein expression by western blot in those colon cancer cell lines and their exosomes isolated from culture supernatants. All four cell lines and their exosomes expressed c-MET/PD-L1 protein at relatively high levels (Fig. 3A–B). Finally, we determined whether the above four cancer cell lines were able to produce xenografts in NOD/SCID mice. The two cell lines HCT116 and SW480 produced strong xenografts models (data not shown) and were selected for use in this study.

To test the effect of the anti-c-MET/PD-1 BsAb on tumor cells migration and invasion, tumor cells were treated with or without the BsAb or JNJ38877605 for 2 h before HGF treatment. The wound healing assay showed that the BsAb significantly suppressed HGF-induced migration of the HCT116 and SW480 tumor cells (Fig. 3C). Furthermore, the matrigel invasion assay showed that both the BsAb and JNJ38877605 inhibited HGF-induced tumor invasion at 24 h timepoint (Fig. 3D). These results indicated that the BsAb inhibited HGF-stimulated CRC cell migration and invasion.

The BsAb inhibits tumor growthin xenograft models

To determine the therapeutic efficacy *in vivo*, the BsAb was evaluated in an adoptive-transfer xenograft tumor model. Xenograft studies were performed using 5-6 -week-old male NOD/SCID mice (n = 4/per group) by subcutaneous injection of HCT116 cells. One week later, the mice were treated IP with IgG4, anti-PD-1 antibody, or BsAb, or by intragastric gavage with JNJ38877605. As shown in Fig. 4A–C, the PBMC + BsAb treatment significantly inhibited tumor size compared with other treatments. However, the body weights of the mice did not change significantly (Fig. 4D). These data collectively suggest that the BsAb is a more potential inhibitor of tumor growth *in vivo* than the anti-PD-1 antibody or c-MET inhibitor.

BsAb inhibits HGF-induced and activation of downstream molecules

The HGF/c-MET signaling pathway plays a significant role in tumor development and metastasis by activating downstream molecules, such as AKT and ERK1/2 [18]. Quercetin and anti-c-MET antibodies inhibit HGF/c-MET signaling by promoting c-MET protein degradation [19]. To clarify whether the BsAb induced c-MET degradation, western blot analysis was performed to assess c-MET stability and expression of c-MET-related downstream molecules. We demonstrated that the BsAb strongly downregulated c-MET protein expression in both dose- and time-dependent manners in HCT116 and SW480 cancer cell lines (Fig. 5A). However, *c-MET* mRNA expression was not affected (data not shown). We also found that HGF-mediated upregulation of phosphorylated c-MET (Tyr1234/5, Tyr12349) was

completely inhibited by BsAb treatment in HCT116 and SW480 cell lines, and the BsAb appeared more efficient than c-MET inhibitor (Fig. 5B).

Phosphorylated c-MET can recruit adaptor protein Grb2-associated binding protein 1 (Gab1), phosphorylates Gab1 at tyrosine site 307, and activate focal adhesion kinase (FAK) [19]. Activation of FAK pathway results in increased cell motility, migration and invasion [20]. To determine if the BsAb inhibited downstream targets of c-MET, HCT116 and SW480 cells were treated with0.5 μM BsAb for 24 h and the whole cell lysates were prepared for western blot analyses. We found that the levels of phosphorylated Gab1 at tyrosine 307 were reduced in both HCT116 and SW480 cells, and the activation of FAK was inhibited by BsAb treatment (Fig. 5C). These data demonstrate that Gab1 and FAK, which are downstream targets of c-MET, may also play an essential role in CRC cell proliferation, migration and invasion, and the BsAb may prove to be an effective inhibitor of cancer development via c-MET targeting.

BsAb inhibits pro-inflammatory cytokines secretion and promotes phagocytose in M2 macrophage

THP1 cells were pretreated with phorbol myristate acetate (50 ng/mL) for 48 h, and differentiated into M1 macrophages (after treatment with LPS, IFN-γ, and IL-6) or M2 macrophages (after treatment with IL-4, IL-6, and IL-13). Real time PCR revealed a significant decrease in the mRNA levels of the M2 macrophages marker *CD163* and *CD206* (*MRC1*) after BsAb treatment ($P < 0.05$) (Fig. 6A). Western blot analysis revealed a significant decrease in PD-1 expression in macrophages after BsAb treatment (Fig. 6B).

M2 macrophages can inhibit T-cell proliferation and activation by secreting immunosuppressive factors, such as C-C motif chemokine ligand 22 (CCL22), interleukin (IL)-10, and transforming growth factor-β, and by recruiting regulatory T cells to tumor tissues. Therefore, M2 macrophages can indirectly promote tumor development by dampening the antitumor immune response [21]. To determine whether the BsAb could inhibit M2 macrophages-mediated secretion of immunosuppressive factors, M2 macrophages were treated with 0.5 μM BsAb for 24 h, and the cell and supernatant were prepared for RT-PCR and ELISA analysis, respectively. The levels of IL-10 and CCL17 (anti-inflammatory factors) were significantly inhibited, while the levels of IL-6 and IL-12 (pro-inflammatory factors) were significantly increased when M2 macrophages were treated with BsAb ($P < 0.05$) (Fig. 6C, D). Additionally, the phagocytic function of M2 macrophages, as determined by the neutral red assay, was significantly enhanced after BsAb treatment (Fig. 6E). Thus, BsAb blockade shifts the balance of anti-inflammatory M2 macrophages toward activated antitumorigenic M1 macrophages, which may also play an important role in its therapeutic efficacy.

The clinical value of plasma exosomes containing c-MET/PD-L1 for CRC

The exosomes from CRC patient plasma were successfully isolated by differential centrifugation, and size, morphology, and specific markers were verified. Morphologically, exosomes were spherical, membrane-bound vesicles (Fig. S4A). Nanoparticle tracking analysis demonstrated that the mode size of the exosomes was approximately 100 nm (Fig. S4B), and western blotting analysis detected expression of exosomal specific markers (flotilin-1, TSG101, and CD9) (Fig. S4C).

ELISAs were used to measure the secretion of c-MET and PD-L1 in plasma and plasma exosomes from CRC patients. There was no correlation between the plasma levels of c-MET or PD-L1 and tumor stages (Fig. 7A). However, the levels of plasma exosomal c-MET and PD-L1 positively correlated with tumor stages , and (Fig. 7B). Among the four parameters tested, the ROC curve indicated that the level of plasma exosomal c-MET best distinguished CRC patients from healthy controls (Fig. 7C).

Discussion

The c-MET expression pattern provides a strong rational for targeted antibody therapy, although several attempts to produce antibody therapeutics against c-MET have failed [22–24]. Traditional bivalent antibodies often cause c-MET auto-activation because of antibody-mediated c-MET dimerization. Several antibodies have been developed in past years that avoid antibody-induced c-MET activation, such as emibetuzumab and onartuzumab [25–27]. However, the clinical development of c-MET-targeted antibodies has been challenging. Additionally, anti-HGF antibodies have been evaluated in clinical trials, including the monoclonal antibodies rilotumumab and ficlatuzumab [28–29]. These antibodies inhibit HGF/c-MET binding; however, both failed to improve clinical outcomes. Therefore, the sole inhibition of HGF/c-MET signaling does not appear to be sufficient to achieve clinical efficacy. Emerging evidence indicates that the abnormal expression of immune cell surface antigens contribute to tumor evasion in the tumor microenvironment. To resolve the above problems, an antibody that can simultaneously target tumor cells and avoid inactivation of immune cells has great potential value. We designed a novel BsAb that binds to only one c-MET and one PD-1 proteins target. The monovalent nature of this BsAb avoids both the undesired activation of T cells caused by PD-1 cross-linking and induction of c-MET signaling through receptor dimerization in tumor cells. The structure of the PD-1 scFv does not affect the binding activity of c-MET *in vitro* and has a human IgG1 Fc region that extends the drug half-life [16–17].

In this study, we found that our BsAb inhibited HGF-induced growth, invasion, and migration of c-MET-dependent CRC *in vivo* and *in vitro* (Fig. 3–4). Our BsAb induced the degradation of c-MET in colorectal cancer cell types, including HCT-116 and SW480 (Fig. 5A). Furthermore, the BsAb inhibited HGF-stimulated c-MET autophosphorylation of Tyr1234/1235 in the activation loop, which activates downstream molecules, such as Gab1 and FAK (Fig. 5B–C). From the above results, we propose that the BsAb may inhibit the HGF/c-MET signaling pathway.

PD-1 expression inhibits numerous immune cell subsets in the tumor microenvironment, including T cells, macrophage, B cells, NK cells, and dendritic cells [30–32]. In a previous study, we found that the BsAb restored cytokine secretion by activated T cells via interaction with PD-1, which may have blocked PD-L1/PD-1 signaling [16]. It was reported that PD-1 expression on the surface of tumor-associated macrophages (TAMs) correlated with decreased phagocytosis; however, PD-L1 removal increased PD-1$^+$ TAM phagocytosis *in vivo* and decreased tumor burden, which suggested that TAM function was rescued [33]. It is unknown if the BsAb plays a role in TAMs function in the tumor microenvironment. In this study, we demonstrated that TAM-mediated anti-tumor immunity could be modulated by the BsAb. The expression levels of CD163, CD206, and PD-1 decreased after BsAb treatment of M2 macrophages,

suggesting that the BsAb treatment increased antitumor M1 macrophages function. We also found that PD-1 positive M2 macrophages promoted the secretion of IL-10 and CCL-17 and inhibited the secretion of TNF-α, IL-1β, IL-6, and IL-12, and BsAb treatment reversed these functions in M2 macrophages. A higher proportion of PD-1 positive TAMs may increase tumor progression, and expression of PD-1 on the surface of M2 macrophages may inhibit phagocytosis; however, our BsAb was able to restore phagocytosis. We hypothesize that these novel mechanisms of action provide a strong rationale for clinical translation of this BsAb for the treatment of CRC patients to improved clinical outcomes.

It is crucial to validate markers during the clinical development of targeted therapies for cancer patients. At present, immunohistochemical detection of PD-L1 expression in tumor tissues has become the primary detection indicator for predicting efficacy, monitoring treatment, and screening patients who benefit from clinical therapeutics that target the PD-L1/PD-1 pathway [34]. Compared with patients who presented with negative/weak PD-L1 expression in their tumors, the response rate of patients with high PD-L1 expression rose from 8–30% [35]. However, the predictive role of PD-L1 expression in tumor tissue is still a matter of debate. Cancers with low expression of PD-L1 may respond to the anti-PD-1 antibody nivolumab, and survival was reported to be longer for nivolumab-treated patients than for those treated with chemotherapy [36]. Chen et al. found that PD-L1 protein can be specifically expressed in exosomes of some tumor patients, which may improve detection [37]. In the MC38 murine tumor model, both exosomal and cellular PD-L1 proteins play an important role in promoting tumor progression, and these mice are sensitive to anti-PD-L1 therapy [38]. Hence, exosomal PD-L1 protein may be a biomarker for clinical immunotherapy that can be detected in patient blood prior to therapy. However, the expression level of secretory exosomal PD-L1 protein in patients with CRC has not been thoroughly studied. In this study, we found that the level of plasma exosomal PD-L1 positively correlated with tumor stages , , and . Furthermore, the level of plasma exosomal PD-L1 distinguished CRC patients from healthy controls. These results suggested that PD-L1 levels in exosomes, but not plasma, were associated with disease progression in CRC patients. Therefore, circulating PD-L1 exosomes may be a useful biomarker to predict the efficacy of BsAb treatment of CRC patients.

In clinical studies, a number of methodologies have been adopted for the evaluation of c-MET overexpression, including determination of gene copy number with fluorescent in-situ hybridization or evaluation of c-MET protein expression using immunohistochemistry [39]. It is important to find simple, sensitive, non-invasive, and reliable biomarkers for c-MET expression in CRC. Peinado et al. reported that blood-derived exosomes from patients with metastatic melanoma contained c-MET protein, which may represent a useful, novel marker for metastatic melanoma patients [40]. However, it has not been reported whether patients with CRC also have secreted exosomes containing c-MET protein or whether these exosomes can be used as a biomarker to predict therapeutic efficacy and monitor treatment of CRC patients. In this study, several databases were used to analyze the expression of c-MET in different tumors and adjacent normal tissues. The results showed that the expression level of c-MET were significantly higher in multiple cancer tissues when compared with levels in the corresponding adjacent tissues, such as COAD and READ. We also found c-MET expression differences between normal and tumor tissues from patients with lymphoid neoplasm diffuse large B-cell lymphoma, brain lower grade

glioma, skin cutaneous melanoma, testicular germ cell tumors, and thymoma. Additionally, there were significant difference in *c-MET* gene expression between COAD and READ tissues and matched adjacent tissues. The resulting diagnostic test showed that there were significant changes in *c-MET* gene expression level in COAD and READ. The levels of c-*MET* gene were higher in M, N, and T stages of tumors compared with levels in the respective normal tissues. Immunohistochemistry validation analysis of those specimens revealed that all tumor cells were c-MET positive with scores of 1–3^{+}, whereas cells in the adjacent tissues were negative, suggesting that c-MET overexpression is tumor-cell specific. In the clinical setting, the results showed that there was no correlation between the level of plasma c-MET and tumor stages (Fig. 7A). The level of plasma exosomal c-MET positively correlated with tumor stages ， ， and (Fig. 7B). The ROC curve showed that, among the four parameters tested, the level of plasma exosomal c-MET best distinguished CRC patients from healthy controls (Fig. 7C).

A better understanding of exosomes expressing the surface proteins c-MET and PD-L1 is required to predict patient response and improve BsAb treatment efficacy. A higher level of circulating c-MET and PD-L1 positive exosome may suggest that treatment with our BsAb may be beneficial. Our studies suggest that CRC cells release c-MET/PD-L1-positive exosome into the tumor microenvironment and circulation to improve anti-tumor immunity systemically. The level of circulating exosomal c-MET and PD-L1 positively correlated with the stages and may provide useful information regarding the response to treatment with our BsAb.

In the tumor microenvironment, BsAb can not only directly target the c-MET antigen in tumor cells and exosome, it but also target the PD-1 antigen expressed by T cells and TAMs, which weakens the inhibitory effect of PD-L1 expressed by tumor cells and free PD-L1 exosomes in the systemic immune system (Fig. 8). Therefore, it has the anti-tumor effect of killing two birds with one stone. In the future, it will be necessary to continue the evaluation of this BsAb using other pre-clinical platform, which may ultimately lead to clinical trials. In addition, this study demonstrates the potential of engineered bispecific antibodies, which and be generated to target other tumor-specific antigens.

We demonstrated the anti-tumor efficacy of our BsAb both *in vitro* and *in vivo* models. The BsAb induced the degradation of c-MET, inhibited HGF-stimulated c-MET autophosphorylation of Tyr1234/5 and Tyr1349 in the activation loop, and reduced downstream activation of Gab1 and FAK. The BsAb reversed polarization and increased phagocytosis of macrophages. These effects are, at least in part, because of the inhibition of HGF/c-MET and PD-L1/PD-1 signaling pathways. With this potential, this BsAb could be developed as a therapeutic candidate for the treatment of patients with c-MET/PD-L1^{+} CRC.

Declarations

Acknowledgments We thank Susan Zunino, PhD, from Liwen Bianji (Edanz) (www.liwenbianji.cn), for editing the English text of a draft of this manuscript.

Funding This work was supported by the National Natural Science Foundation of China (81974314, 82072362, 82002223, 82002222), the Natural Science Foundation of Shanghai (19ZR1448800), the Science and Technology Innovation Action Plan of Shanghai Science and Technology Commission (19411964800, 20YF1443700), the Postdoctoral Science Foundation of China (2020M681399, 2020M681400), Shanghai Public Health System Construction Three-Year Action Plan (2020-2022) Key Disciplines (GWV-10.1-XK04), Shanghai Municipal Health and Health Commission (20204Y0070), the Project supported by Clinical Research Project of Tongji Hospital of Tongji University [ITJ(ZD)1905].

CRediT authors's contribution statement The work presented here was carried out in collaboration among all authors. Zujun Sun conceived and jointly designed the study with Dong Li. Chenzheng Gu and Xuan Wang conducted this study and drafted this manuscript. Anquan Shang, Junlu Wu and Ping Ji analyzed the data. Yiwen Yao and Wenqiang Quan performed experiments. Wenfang Liu revised the manuscript. All authors read and approved the final manuscript.

Conflicts of interest statement The authors declare that they have no competing interests.

References

1. Ferlay J, Soerjomataram I, Dikshit R, Eser S, Mathers C, Rebelo M, et al (2015). Cancer incidence and mortality worldwide: sources, methods and major patterns in GLOBOCAN 2012. Int J Cancer. 136: E359-386.
2. Gong YM, Wu CX, Zhang ML, Peng P, Gu K, Bao PP, et al (2015). Colorectal cancer survival analysis in major areas in Shanghai, China. Chinese Oncology. 25: 497–504.
3. Goel G, Sun W. (2015). Novel approaches in the management of pancreaticductal adenocarcinoma: potential promises for the future. J Hematol Oncol. 8:1–16.
4. Nunez-Prado N, Compte M, Harwood S, Alvarez-Mendez A, Lykkemark S, Sanz L, et al (2015). The coming of age of engineered multivalent antibodies. Drug Discov Today. 2:588–594.
5. Spellman A, Tang SC. (2016). Immunotherapy for breast cancer: past, present, and future. Cancer Metastasis Rev. 35:525–546.
6. Page DB, Postow MA, Callahan MK, Allison JP, Wolchok JD. (2014). Immune modulation in cancer with antibodies. Annu Rev Med. 65:185–202.
7. Topp MS, Gökbuget N, Zugmaier G, Klappers P, Stelljes M, Neumann S, et al (2014). Phase II trial of the anti-CD19 bispecific T cell-engager blinatumomab shows hematologic and molecular remissions in patients with relapsed or refractory B-precursor acute lymphoblastic leukemia. J Clin Oncol. 32: 4134–4140.
8. Spiess C, Zhai Q, Carter PJ. (2015). Alternative molecular formats and therapeutic applications for bispecific antibodies. Mol Immunol. 67:95–106.
9. Fan D, Li W, Yang Y, Zhang X, Zhang Q, Yan Y, et al (2015). Redirection of CD4 + and CD8 + T lymphocytes via an anti-CD3× anti-CD19 bi-specific antibody combined with cytosine arabinoside

and the efficient lysis of patient derived B-ALL cells. J Hematol Oncol. 8:108.

10. Wang S, Chen C, Meng Y, Hu S, Zheng L, Song J, et al (2012). Effective suppression of breast tumor growth by an anti-EGFR/ErbB2 bispecific antibody. Cancer Lett. 325:214–219.
11. Grugan KD, Dorn K, Jarantow SW, Bushey BS, Pardinas JR, Laquerre S, et al. (2017). Fc-mediated activity of EGFR x c-Met bispecific antibody JNJ-61186372 enhanced killing of lung cancer cells. MAbs. 9:114–126.
12. Tao JJ, Castel P, Radosevic-Robin N, Elkabets M, Auricchio N, Aceto N, et al (2014). Antagonism of EGFR and HER3 enhances the response to inhibitors of the PI3K/Akt pathway in triple-negative breast cancer. Sci Signal. 7:1–19.
13. Fitzgerald JB, Johnson BW, Baum J, Adams S, Ladevaia S, Tang J, et al (2014). MM-141, an IGF-IR- and ErbB3-dricted bispecific antibody, overcomes network adaptations that limit activity of IGF-IR inhibitors. Mol Cancer Therap. 13:410–425.
14. Herbst RS, Soria JC, Kowanetz M, Fine GD, Hamid O, Gordon MS, et al (2014). Predictive correlates of response to the anti-PD-L1 antibody MPDL3280A in cancer patients. Nature. 515:563–567.
15. You H, Ding W, Dang H, Jiang Y, Rountree CB, et al (2011). c-Met represents a potential therapeutic target for personalized treatment in hepatocellular carcinoma. Hepatology. 54:879–889.
16. Sun ZJ, Wu Y, Hou WH, Wang YX, Yuan QY, Wang HJ, Yu M. (2017). A novel bispecific c-Met/PD-1 antibody with therapeutic potential in solid cancer. Oncotarget. 8:29067–29079.
17. Wu Y, Yu M, Sun Z, Hou W, Yan Y, Yuan Q, Mo W. (2017). Generation and characterization of a bispecific antibody targeting both PD-1 and c-Met. Protein Pept Lett. 24:1–8.
18. Steinway SN, Dang H, You H, Rountree CB, Ding W. (2015). The EGFR/ErbB3 pathway acts as a compensatory survival mechanism upon c-Met inhibition in human c-Met + hepatocellular carcinoma. PLoS One. 10:1–16.
19. Cao HH, Cheng CY, Su T, Fu XQ, Guo H, Li T, et al (2015). Quercetin inhibits HGF/c-Met signaling and HGF-stimulated melanoma cell migration and invasion. Mol Cancer. 14:103–114.
20. Birchmeier C, Birchmeier W, Gherardi E, Vande Woude GF. (2003). Met, metastasis, motility and more. Nat Rev Mol Cell Biol. 2003;4:915–925.
21. Kryczek I, Zou L, Rodriguez P, Zhu GF, Wei S, Mottram P, et al (2006). B7-H4 expression identifies a novel suppressive macrophage population in human ovarian carcinoma. J Exp Med. 203:871–81.
22. Heukers R, Altintas I, Raghoenath S, Zan ED, Pepermans R, Roovers RC, et al (2014). Targeting hepatocyte growth factor receptor (Met) positive tumor cells using internalizing nanobody-decorated albumin nanoparticles. Biomaterials.35:601–610.
23. Su Z, Han Y, Sun Q, Wang XX, Xu T, Xie W, et al (2019). Anti-MET VHH pool overcomes MET-targeted cancer therapeutic resistance. Mol Cancer Ther. 18:100–111.
24. Gherardi E, Birchmeier W, Birchmeier C, Vande Woude G. (2012). Targeting MET in cancer: rationale and progress. Nat Rev Cancer. 12:89–103.

25. Rosen LS, Goldman JW, Algazi AP, Turner PK, Moser B, Hu T, et al (2017). A first-in-human phase â study of a bivalent MET antibody, emibetuzumab (LY2875358), as monotherapy and in combination with erlotinib in advanced cancer. Clin Cancer Res. 23:1910–1919.
26. Spigel DR, Ervin TJ, Ramlau RA, Daniel DB, Goldschmidt JH Jr, Blumenschein GR Jr, et al. (2013). Randomized Phase II trial of Onartuzumab in combination with erlotinib in patients with advanced non-small-cell lung cancer. J Clin Oncol. 31:4105–4114.
27. Merchant M, Ma X, Maun HR, Zheng Z, Peng J, Romero M, et al (2013). Monovalent antibody design and mechanism of action of onartuzumab, a MET antagonist with anti-tumor activity as a therapeutic agent. Proc Nat Acad Sci. 110:E2987-2996.
28. Burgess TL, Sun J, Meyer S, Tsuruda TS, Sun J, Elliott G, et al (2010). Biochemical characterization of AMG 102: a neutralizing, fully human monoclonal antibody to human and nonhuman primate hepatocyte growth factor. Mol Cancer Ther. 9:400–409.
29. D'Arcangelo M, Cappuzzo F. (2013). Focus on the potential role of ficlatuzumab in the treatment of non-small cell lung cancer. Biologics. 7:61–68.
30. Gordon SR, Maute LR, Dulken BW, Hutter G, George BM, McCracken MN, et al (2017). PD-1 expression by tumor-associated macrophages inhibits phagocytosis and tumor immunity. Nature. 545:459–499.
31. Benson DM, Bakan CE, Mishra A, Hofmeister CC, Efebera Y, Becknell B, et al (2010). The PD-1/PD-L1 axis modulates the natural killer cell versus multiple myeloma effect: a therapeutic target for CT-011, a novel monoclonal anti-PD-1 antibody. Blood. 116:2286–2294.
32. Karyampudi L, Lamichhane P, Krempski J, Kalli KR, Behrrns MD, Vargas DN, et al. (2016). PD-1 blunts the function of ovarian tumor-infiltrating dendritic cells by inactivating NF-κB. Cancer Res. 76:239–250.
33. Gordon SR, Maute RL, Dulken BW, Hutter G, George BM, McCracken MN, et al (2017). <background-color:#CCCCFF;uvertical-align:super;>PD-1 expression</background-color:#CCCCFF;uvertical-align:super;> by <background-color:#CCCCFF;uvertical-align:super;>tumor-associated macrophages inhibits phagocytosis</background-color:#CCCCFF;uvertical-align:super;> and <background-color:#CCCCFF;uvertical-align:super;>tumor immunity</background-color:#CCCCFF;uvertical-align:super;>. Nature. 545:495–499.
34. Ilie M, Long-Mira E, Bence C, Butori C, Lassalle S, Bouhlel L, et al (2016). Comparative study of the PD-L1 status between surgically resected specimens and matched biopsies of NSCLC patients reveal major discordances: a potential issue for anti-PD-L1 therapeutic strategies. Ann Oncol. 27:147–153.
35. Mezquita L, Auclin E, Ferrara R, Charrier M, Remon J, Planchard D, et al (2018). Association of the lung immune prognostic index with immune checkpoint inhibitor outcomes in patients with advanced non-small cell lung cancer. JAMA Oncol. 4:351–357.
36. Borghaei H, Paz-Ares L, Horn L, Spigel DR, Steins M, Ready NE, et al. (2015). Nivolumab versus docetaxel in advanced nonsquamous non-small-cell lung cancer. N Engl J Med. 373:1627–1639.
37. Chen G, Huang AC, Zhang W, Zhang G, Wu M, Xu W, et al. (2018). Exosomal PD-L1 contributes to immunosuppression and is associated with anti-PD-1 response. Nature. 560:382–386.

38. Poggio M, Hu T, Pai C, Chu B, Belair CD, Chang A, et al (2019). Suppression of exosomal PD-L1 induces systemic anti-tumor immunity and memory. Cell. 177:414–427.
39. Koeppen H, Rost S, Yauch RL. (2014). Developing biomarkers to predict benefit from HGF/MET pathway inhibitors. J Pathol. 232:210–218.
40. Peinado H, Alekovi M, Lavotshkin S, Matei I, Costa-Silva B, Moreno-Bueno G, et al (2012). Melanoma exosomes educate bone marrow progenitor cells toward a pro-metastatic phenotype through MET. Nat Med. 18: 883–891.

Tables

Table 1. Clinical characteristics of CRC patients

Characteristics	Total (N)	%
Age (years)		
<65	21	65.7
≥65	11	34.3
Gender		
Male	19	59.4
Female	13	40.6
Hisology		
Colon	32	100
TNM Stage		
	7	21.9
	6	18.75
	13	40.6
	6	18.75
Tumor Size (cm)		
≤2.5	15	46.9
2.5	17	53.1
Distant Metastasis		
M0	26	81.25
M1	6	18.75

Table 2. The correlation between c-MET expression and pathological stages

Characteristics	Low expression of c-MET	High expression of c-MET	p
n	239	239	
T stage, n (%)			0.803
T1	4 (0.8%)	7 (1.5%)	
T2	43 (9%)	40 (8.4%)	
T3	161 (33.8%)	162 (34%)	
T4	31 (6.5%)	29 (6.1%)	
N stage, n (%)			0.766
N0	143 (29.9%)	141 (29.5%)	
N1	51 (10.7%)	57 (11.9%)	
N2	45 (9.4%)	41 (8.6%)	
M stage, n (%)			0.572
M0	175 (42.2%)	174 (41.9%)	

Table 3. Univariate and multivariate analysis the expression of c-MET

Characteristics	Total (N)	Univariate analysis		Multivariate analysis	
		Hazard ratio (95% CI)	P value	Hazard ratio (95% CI)	P value
T stage (T3&T4 vs. T1&T2)	476	3.072 (1.423-6.631)	0.004	4.080 (1.258-13.237)	0.019
N stage (N1&N2 vs. N0)	477	2.592 (1.743-3.855)	<0.001	1.455 (0.884-2.394)	0.14
M stage (M1 vs. M0)	414	4.193 (2.683-6.554)	<0.001	2.868 (1.718-4.787)	<0.001
c-MET (High vs. Low)	477	0.815 (0.553-1.202)	0.302		

Figures

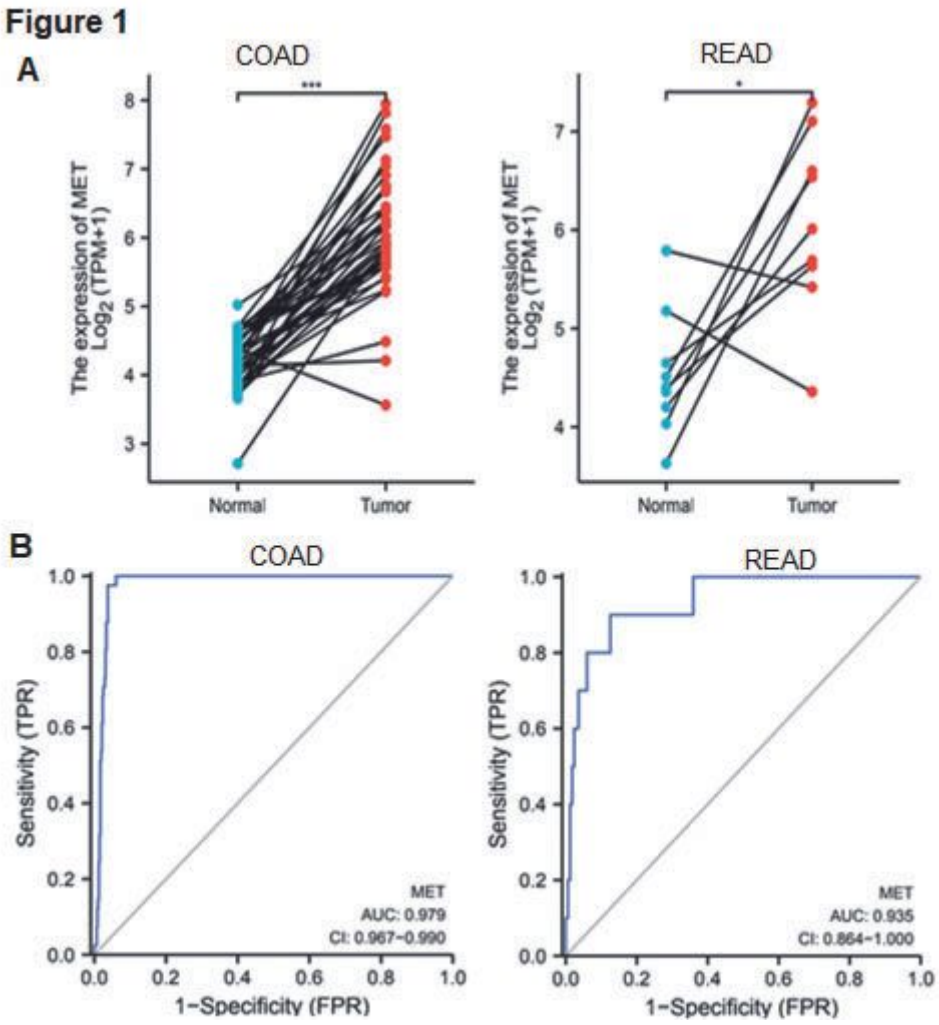

Figure 1

Correlation between *c-MET* gene expression and receiver operating characteristic (ROC) curves for colorectal cancer from the Cancer Genoma Atlas (TCGA). (**A**) The RStudio was used to perform *MET* gene expression analysis of colon adenocarcinoma (COAD) and rectum adenocarcinoma (READ) and matched adjacent tissues from TCGA database. (**B**) ROC curve was used to analyze the changes in *MET* gene expression levels for COAD and READ from the TCGA database A. **P* < 0.05; ****P* < 0.001.

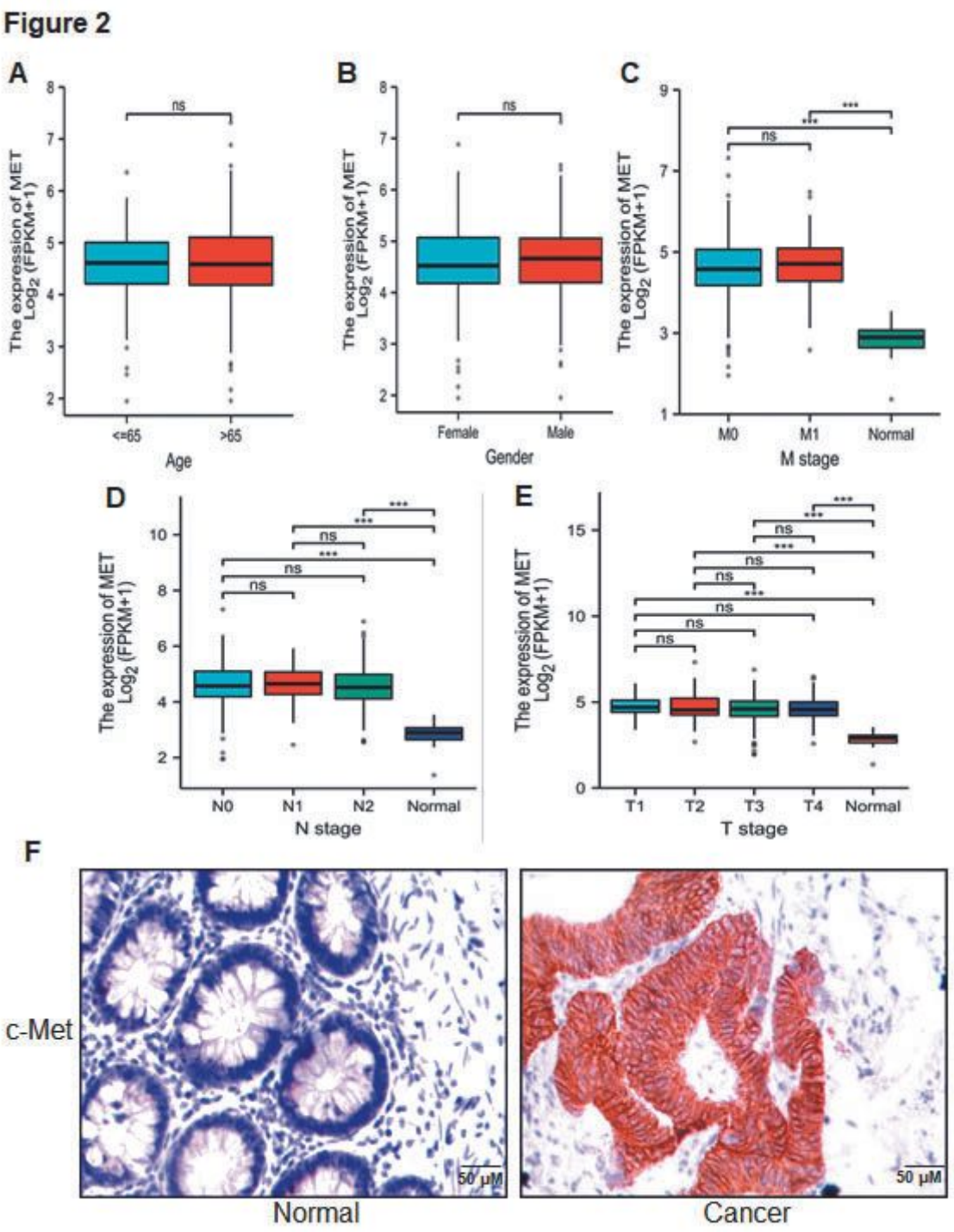

Figure 2

The Correlations between *c-MET* gene expression and pathological stages in colorectal cancer patients. (**A**) Age. (**B**) Gender. (**C**) M stage. (**D**) N stage. (**E**) T stage. (**F**) Immunohistochemistry staining was performed on paraffin-embedded colorectal cancer and tissues. **P* < 0.05; ***P* < 0.01; ****P* < 0.001.

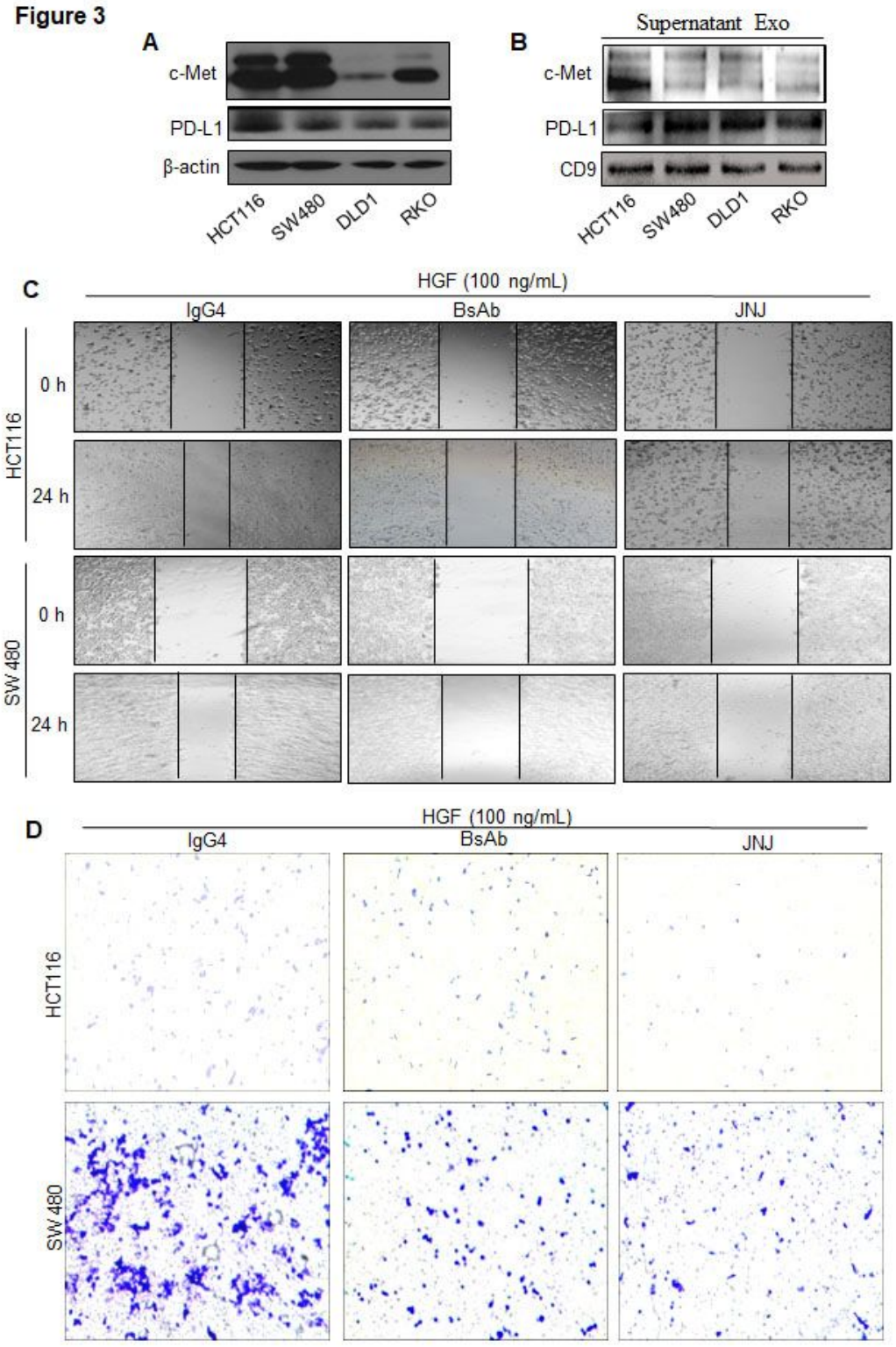

Figure 3

The anti-c-MET/PD-1 BsAb inhibits HGF-induced colorectal cancer cell migration and invasion. (**A**) c-MET and PD-L1 protein expression was detected in colon cancer cell lines by western blot analysis. (**B**) c-MET and PD-L1 protein expression was detected in exosomes isolated from colon cancer cell culture supernatants by western blot analysis. (**C**) Wound healing assay. Cancer cells were cultured to confluency in 24-well plates. A linear scrape wound was created using a sterile pipette tip and the cells were treated

with the indicated concentrations of BsAb or JNJ38877605 and 100 ng/mL HGF for 24 h (original magnification, 100×). (**D**) Tumor invasion assay using a matrigel basement membrane matrix. Cancer cells were treated with the BsAb or JNJ38877605 for 24 h with 100 ng/mL HGF was added to the lower chamber. Data are presented as mean ± SD from three independent experiments.

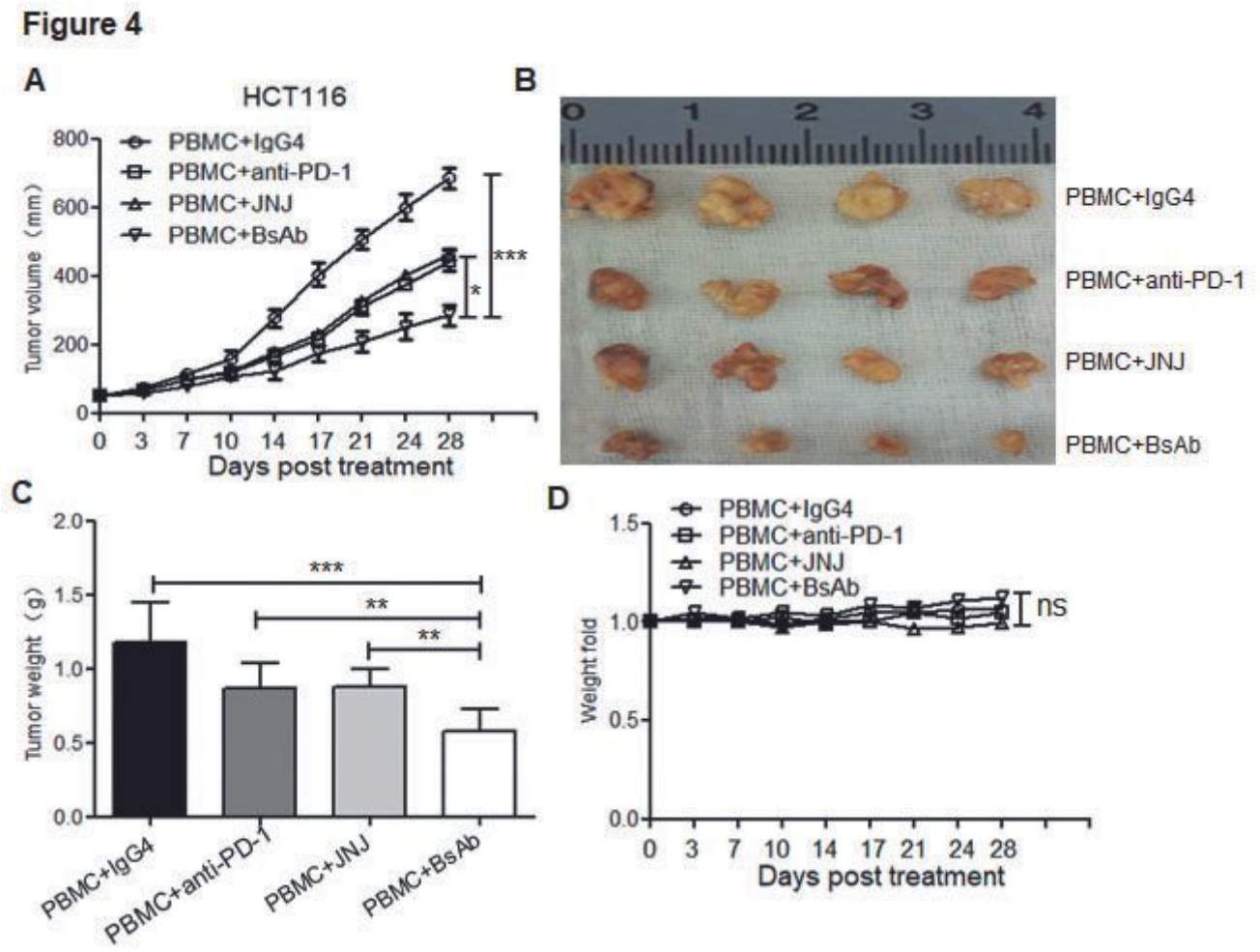

Figure 4

The BsAb inhibits NOD/SCID mice xenografted with the HCT116 CRC cell lline. (**A**) Tumor volumes measured on indicated days are shown for the BsAb treatment and control groups. (**B**) HCT116 tumor xenografts were removed 4 days after the last treatment. (**C**) Weight of xenografted tumors. (**D**) Folds change in body weights of the mice in each treatment group. Data represent the mean ± SD of 4 individual mice per group. $^{**}P < 0.01$; $^{***}P < 0.001$.

Figure 5

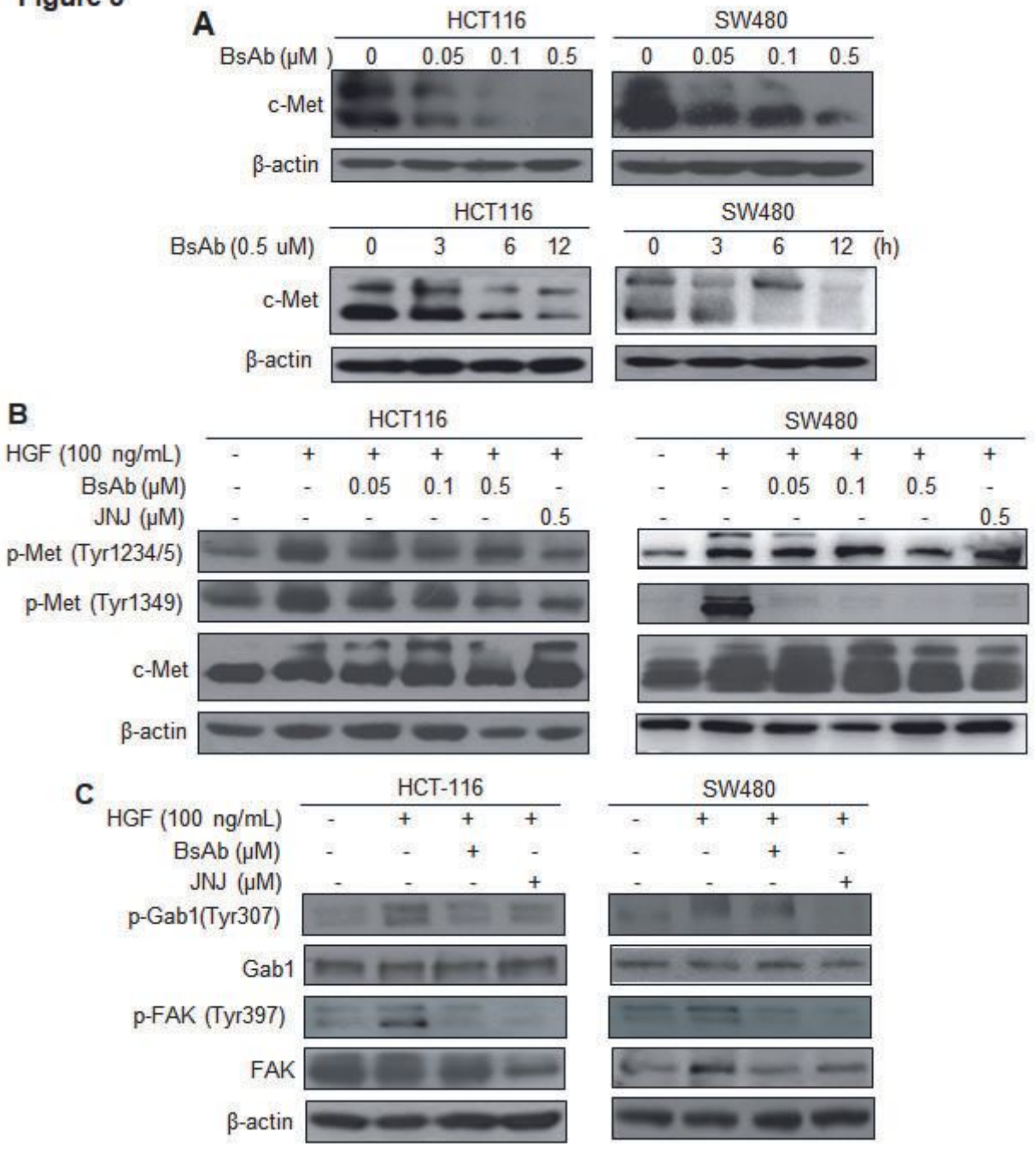

Figure 5

The BsAb promotes c-MET degradation and inhibits hepatocyte growth factor (HGF)-triggered c-MET and its downstream targets. (**A**) The BsAb promotes c-MET degradation. (**B**) The BsAb inhibits HGF-triggered c-MET activation. (**C**) The BsAb inhibits HGF-triggered c-MET downstream targets activation.

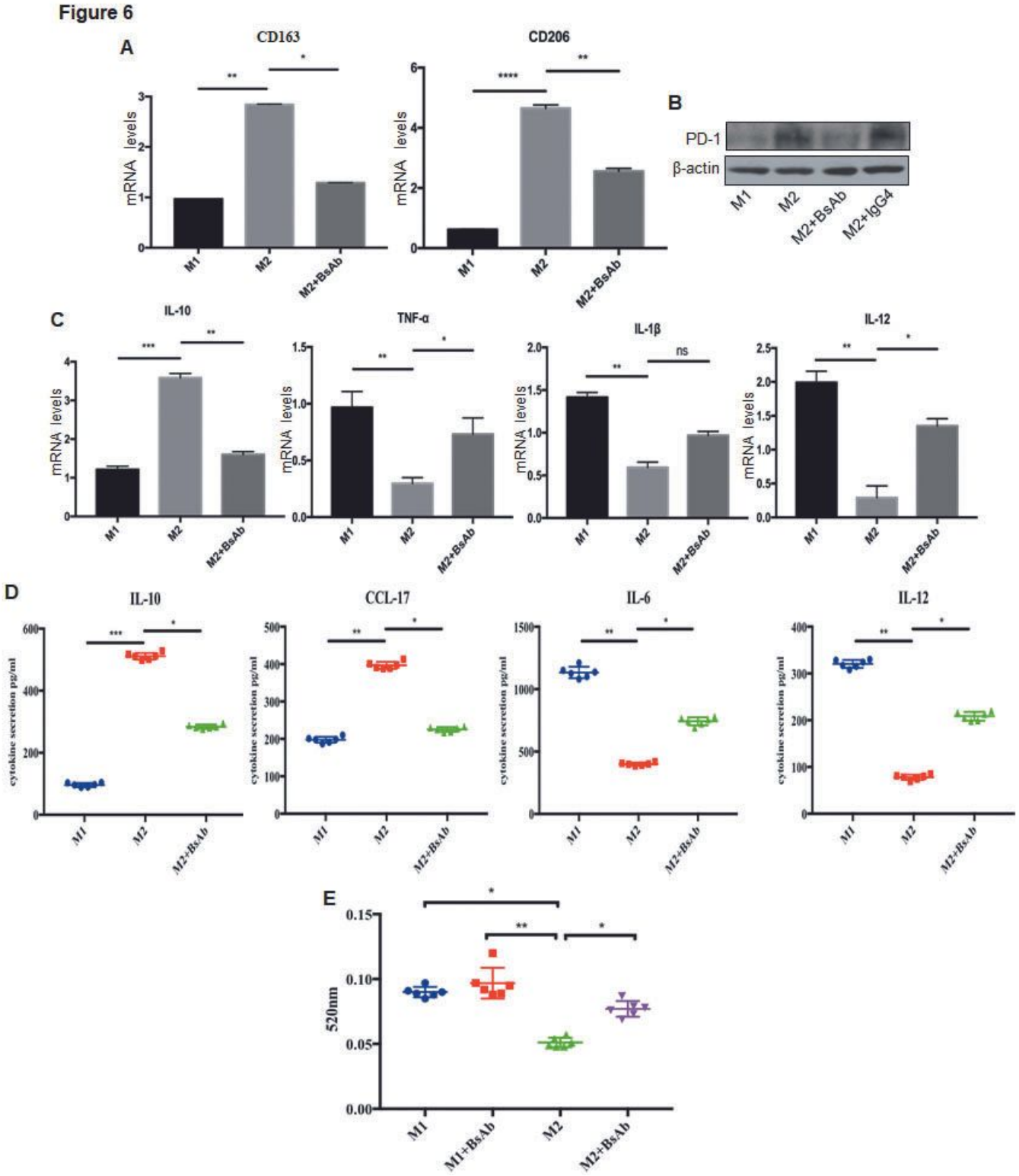

Figure 6

The BsAb inhibits anti-inflammatory cytokines secretion and promotes phagocytose of M2 macrophage. (**A**) The relative mRNA expression of *CD163* and *CD206* detected by qPCR. (**B**) The expression of PD-1 detected by western blot. (**C**) The expression of cytokine mRNA detected by qPCR. (**D**) Enzyme-linked immunosorbent assay. (**E**) The phagocytic function detected by the neutral red assay. The assays were

repeated three times and each sample had 3 holes. The results were presented as mean ± SD. *$P < 0.05$, **$P < 0.01$, ***$P < 0.001$.

Figure 7

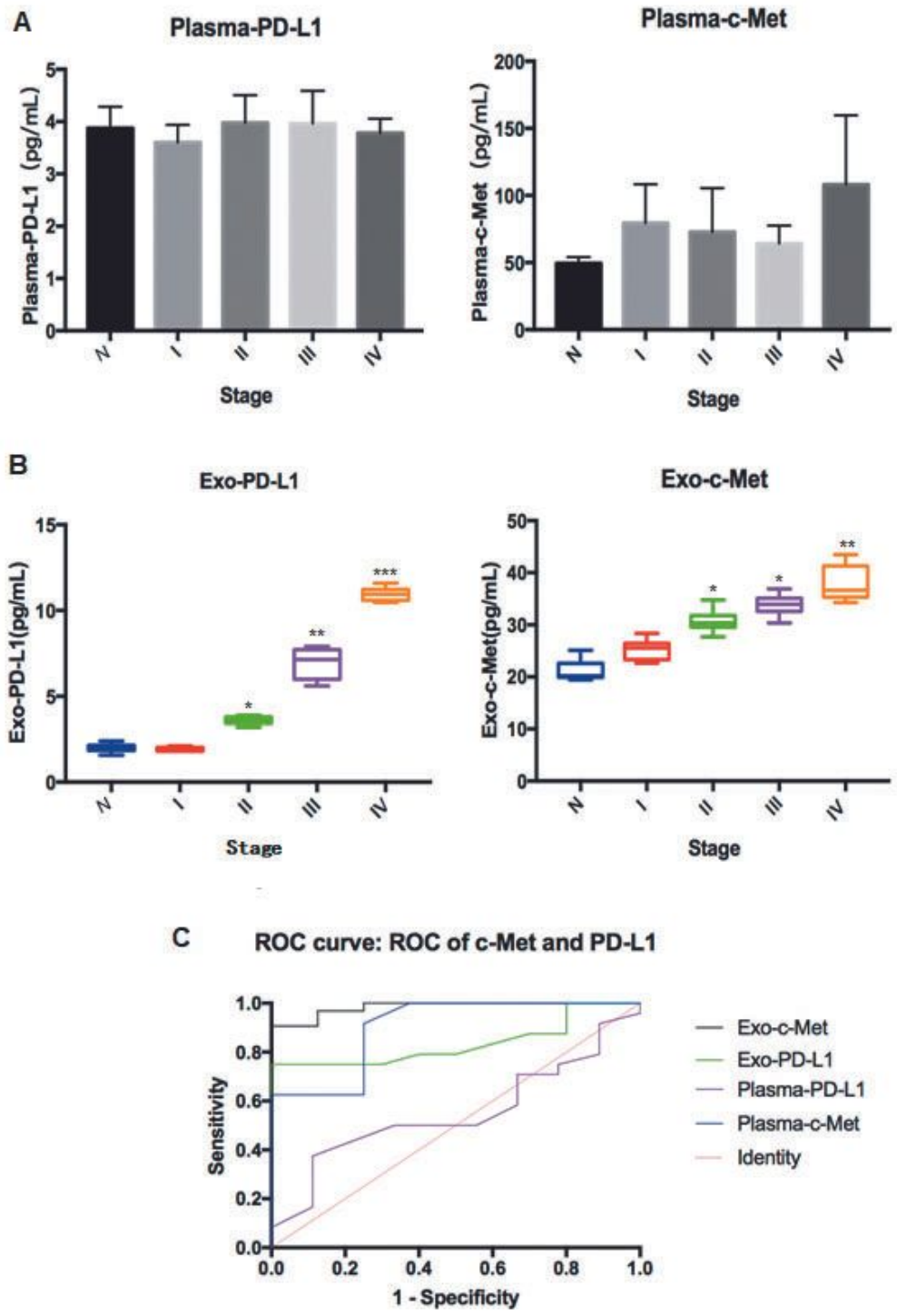

Figure 7

The PD-L1 and c-MET expression levels and clinical value of plasma exosome from CRC patients. (**A**) ELISA detected the circulating levels of plasma PD-L1 and c-MET proteins in CRC patients and healthy

controls. (**B**) ELISA detected the levels of plasma exosomal PD-L1 and c-MET proteins in CRC patients and healthy controls. (**C**) Receiver operating characteristic (ROC) curve analysis shows the clinical value of the indicated parameters for CRC. Data represent the mean ± SD for three experiments. *$P < 0.05$; **$P < 0.01$; ***$P < 0.001$.

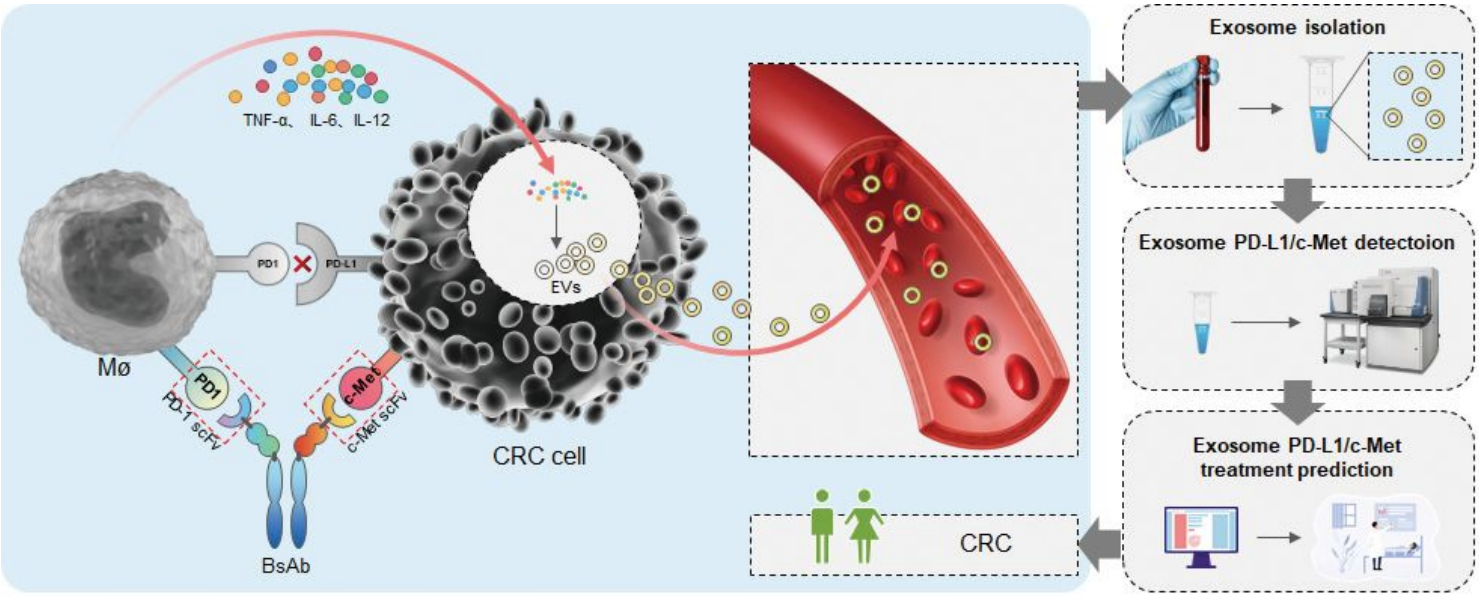

Figure 8

Schematic cartoon of mechanism of BsAb as a therapeutic candidate for the treatment of patients with c-MET/PD-L1^{+} CRC. BsAb binds to macrophages to improve their inflammatory factor secretion and phagocytosis. BsAb binds to c-MET on tumor cells and inhibits its downstream signaling pathway.

Supplementary Files

This is a list of supplementary files associated with this preprint. Click to download.

- SupplementaryData.docx